

Refractive index of carcinogen-induced rat mammary tumours

Adam M Zysk^{1,2}, Eric J Chaney² and Stephen A Boppart^{1,2,3}

¹ Department of Electrical and Computer Engineering, University of Illinois at Urbana-Champaign, Urbana, IL 61801, USA

² Beckman Institute for Advanced Science and Technology, University of Illinois at Urbana-Champaign, Urbana, IL 61801, USA

³ College of Medicine, University of Illinois at Urbana-Champaign, Urbana, IL 61801, USA

E-mail: boppart@uiuc.edu

Received 28 December 2005, in final form 23 February 2006

Published 11 April 2006

Online at stacks.iop.org/PMB/51/2165

Abstract

Near-infrared optical techniques for clinical breast cancer screening in humans are rapidly advancing. Based on the computational inversion of the photon diffusion process through the breast, these techniques rely on optical tissue models for accurate image reconstruction. Recent interest has surfaced regarding the effect of refractive index variations on these reconstructions. Although many data exist regarding the scattering and absorption properties of normal and diseased tissue, no measurements of refractive index appear in the literature. In this paper, we present near-infrared refractive index data acquired from *N*-methyl-*N*-nitrosourea-induced rat mammary tumours, which are similar in pathology and disease progression to human ductal carcinoma. Eight animals, including one control, were employed in this study, yielding data from 32 tumours as well as adjacent adipose and connective tissues.

1. Introduction

1.1. Optical breast imaging

The use of near-infrared (NIR) optical imaging in the investigation of breast disease has undergone rapid growth. The diffusion tomography technique, for example, is of significant interest due to its sensitivity to haemoglobin oxygenation levels. Initially investigated as a screening tool for the identification of lesions within the breast, this technology has also been adapted to augment current imaging modalities by providing a non-invasive means of assessing vascularization and the effects of therapies (Gibson *et al* 2005).

The transport of NIR light through thick tissue specimens, such as a human breast, falls into the diffusion regime, wherein many scattering events are expected to occur. In order to form images by the measurement of diffuse light, reconstruction must be based on the accurate

definition of a light transport model. Inversion of this forward model results in a reconstructed image, but is difficult since the problem is ill-posed and underdetermined. The problem is, therefore, often approached using very large detection arrays and computationally complex reconstruction methods, which have recently demonstrated improvements in resolution (Arridge 1999, Markel and Schotland 2005, Schweiger *et al* 2003). An important factor in the definition of a forward model is the incorporation of *a priori* optical properties of the tissue to be studied. A number of studies have been conducted to assess the scattering and absorption properties of normal and diseased breast tissues both *in vivo* and *in vitro* (Cerussi *et al* 2001, Chernomordik *et al* 2002, Durduran *et al* 2002, Fantini *et al* 1998, Grosenick *et al* 2004, Peters *et al* 1990, Shah *et al* 2004). However, with the exception of a reference in the time-resolved imaging literature (Das *et al* 1997), no investigation of breast tissue refractive index (RI) values appears in the literature.

The importance of RI variations in diffusion tomography image formation is garnering increasing attention. The conventional radiative transport equation, used to describe light propagation in tissue, requires that the refractive index of the tissue be uniform. Since this is presumably not the case in most applications, modifications for spatially varying RI have been made (Ferwerda 1999, Martí-López *et al* 2003, Tualle and Tinetti 2003). The effects of these modified transport equations on image reconstructions have recently been investigated (Dehghani *et al* 2003, 2005). The studies showed that images from tissues with a spatially varying RI that are modelled as having a uniform RI suffer from severe degradation. These adverse effects are, of course, inherently linked to both the magnitude and variation of RI values within the tissue. Unfortunately, however, these studies are based on speculative RI values since no such data exist in the literature.

In addition to diffuse optical imaging of the entire breast, optical techniques that tomographically image smaller tissue areas have also emerged for the treatment of breast disease. Coherence-based techniques such as optical coherence tomography (OCT), for instance, have been investigated for the visualization of tumour margins and may also hold potential for needle biopsy guidance and the detection of lymph node metastases (Boppart *et al* 2004, Iftimia *et al* 2005, Luo *et al* 2005, Zysk and Boppart 2006). The depth sensitivity of the interferometric detection scheme used in OCT has also led to its use as a RI measurement and imaging modality (Alexandrov *et al* 2003, Ohmi *et al* 2000, Tearney *et al* 1995, Sorin and Gray 1992, Wang *et al* 2002, Zysk *et al* 2003, Zvyagin *et al* 2003). Finally, RI has been suggested as a tool for the selective delivery of laser energy to biological tissues in surgical procedures (Domankevitz *et al* 2000).

1.2. Animal model

The most widely used animal model for the study of breast cancer is the *N*-methyl-*N*-nitrosourea (MNU)-induced tumorigenesis in rat mammary tissue. Sexually immature female rats given intraperitoneal injections of MNU rapidly develop tumours at a high rate of incidence with negligible toxicity (Gullino *et al* 1975, McCormick *et al* 1981, Thompson and Adlakha 1991, Thompson *et al* 1992, 1995). The resulting pattern of lesion occurrence and pathological structure is highly consistent with the pathogenesis of human disease (Singh *et al* 2000, Thompson *et al* 2000b). Also, similarities to human disease have been reported in the hormone dependence and immunohistological profile of the lesions. As a result of these similarities, this model has been used to study a wide variety of disease properties and treatments (Clarke 1996, 1997).

The MNU rat tumour model is highly adaptable for specific research studies. By varying the carcinogen dose and number of injections, the incidence, latent period and quantity

of tumours can be adjusted, enabling detailed study of tumourigenesis at different stages (McCormick *et al* 1981, Thompson *et al* 1992, 1995, Thompson and Adlakha 1991). This has led to the study of hormone dependence, genetic expression, drug and dietary therapies, and pathological development using this model.

The majority of MNU-induced rat mammary tumours are hormone dependent and possess abundant oestrogen, progesterone and prolactin receptors (Arafah *et al* 1980). Studies in ovariectomized rats have shown that hormone-dependent progression is conferred at the time of carcinogen injection and that tumourigenesis is both oestrous cycle dependent and highly dependent on the presence of both oestrogen and progesterone (Anderson and Beattie 1992, Arafah *et al* 1982, Bigsby 2002, Thompson *et al* 1998). Long-term studies have also shown that after an initial reduction in size in ovariectomized animals, many tumours lose their dependence on oestrogen receptors and re-develop (Thordarson *et al* 2001). These and other related hormonal studies are of great importance to the study of human breast cancer as is evident from the fact that the clinical emphasis on oestrogen receptor testing for endocrine therapy efficacy prediction in humans was spurred in large part by early studies in rat models (Chang *et al* 2002).

Genetic investigation using the MNU model includes studies showing genetic overexpression (Lu *et al* 1997), possible irreversible deregulation of *Ha-ras-1* expression in initiated cells (Jin *et al* 1996) and age dependence (Sinha *et al* 1983, Thompson *et al* 2000a). Most notably, immunohistochemical and microarray analyses were used to show that the gene expression profiles of rat tumours are classified as non-invasive, ER-positive ductal carcinomas and are similar to human ER-positive, low-to-intermediate grade breast cancer (Chan *et al* 2005).

These aforementioned similarities to human disease have led to the use of the MNU model as a platform for cancer therapy investigations. In addition to chemoprevention studies, the effects of trioxifene, tamoxifen and ovariectomy therapies have been investigated (Green *et al* 1999, Rose *et al* 1981). The potential links between tumour development and dietary fat and cholesterol intake in MNU rat models have also been probed, prompting further investigation into the human dietary links to breast cancer (Bartsch *et al* 1999, Cohen *et al* 1986, Fay *et al* 1997, Welsch 1992). Finally, the relationship between physical activity and cancer development have been studied both in the MNU rat model and in human patients, developing a potential link between exercise and breast cancer incidence (Clarke 1997, Thompson 1997).

Originating from multipotent cells in the terminal end bud, the MNU-induced lesion generally emulates the pathogenesis of human ductal carcinoma (Crist *et al* 1992, Dulbecco *et al* 1986, Thompson *et al* 2000b). *In situ* carcinomas develop as either criboform or papillary disease, and invasive ductal disease is typically characterized by a broad front of stromal invasion. Tumour development is accompanied by angiogenesis but lacks the microcalcifications often present in human disease. Metastasis to the lymph nodes, liver, lung, kidney and spleen has also been observed (Gullino *et al* 1975, Moon *et al* 1977, Singh *et al* 2000, Thompson *et al* 2002). Benign disease may occur, as well, but rats typically develop limited types of benign lesions, including fibroadenoma and papilloma, when compared to humans (Singh *et al* 2000). Additionally, the immunohistological profile of the tumours is also similar to that found in human cancer, developing like spontaneously arising malignancies (Hill *et al* 2004).

It is clear that the use of MNU-induced tumours has become a suitable model for the study of human breast cancer in many cases. Recently, optical imaging studies have also made use of the model for the assessment of breast cancer margins and lymph node architecture (Boppart *et al* 2004, Luo *et al* 2005). The use of MNU-induced rat mammary tumours in

this investigation is, therefore, a natural continuance of these studies and is expected to yield results that correspond well with the properties of human breast disease.

2. Materials and methods

2.1. Tumour induction

Seven female virgin Sprague–Daley rats were given two intraperitoneal injections, at 21 and 35 days of age, with a 12.5 mg ml⁻¹ MNU solution at 55 mg per kg of animal weight. An eighth control rat was not injected. Each animal was housed individually in a temperature- and lighting-controlled environment and fed rodent laboratory chow. The animals were palpated weekly post-injection until a mass was detected, after which they were euthanized via carbon dioxide asphyxiation. All MNU-injected animals developed palpable tumours. The control animal developed no palpable lesions and was euthanized and evaluated after all other animals were processed. Tissue from recently euthanized animals was removed from the mammary tissue extending from the groin, through the abdomen, and to the ventral neck region. A midline and two lateral abdominal incisions were made, exposing the area of interest. Tumours were identified based on gross examination and the size of each mass was recorded. After removal, samples were placed in 0.9% saline solution and refrigerated. The animals used in this study were cared for under protocols approved by the Institutional Animal Care and Use Committee of the University of Illinois at Urbana-Champaign.

2.2. Tissue preparation and classification

After removal from the animal, tissue was immediately placed in a saline solution and refrigerated prior to optical analysis. Tissue was separated into smaller samples, each having an approximate volume of 1 mm³. In an effort to achieve a homogeneous structure within each tissue sample, separation was performed based on visual and tactile investigation of the tissue. Each sample was placed on a glass microscope slide for analysis, which involved exposing the sample to NIR radiation for about 1 min. All optical measurements were taken within 7 h of each animal's death, but on average, analysis took place within 4 h. After optical analysis, each sample was placed in a 10% formalin solution. Finally, samples underwent standard histological processing, including being embedded in paraffin wax, sectioned and stained with haematoxylin and eosin (H&E) for microscopic analysis. Analysis of the histological slides resulted in the classification of each tissue sample as adipose, fibrous stroma or tumour tissue. The inherent nature of any complex biological system dictates that some intermixing of tissue structures will exist. It was necessary, however, that each tissue sample in this study consists of only one tissue type. Therefore, samples that were found to consist of less than 85% of a single tissue type (either tumour, stroma or adipose) upon microscopic evaluation were eliminated from the study, leaving only the data that were measured from highly homogeneous tissue samples. Tumours were also evaluated for the presence of necrotic regions.

2.3. Measurement technique

The measurement of RI was implemented using an interferometric imaging system. Based on an optical coherence tomography (OCT) technique (Tearney *et al* 1995), measurement consisted of the analysis of a cross-sectional OCT image of the sample and a reference object. Typically, the sample was placed on a flat glass microscope slide and imaged using an OCT system (figure 1(a)). Since OCT depends on the matched path length between the two arms of an interferometer, any change in the RI along this path yields a displacement in the resulting

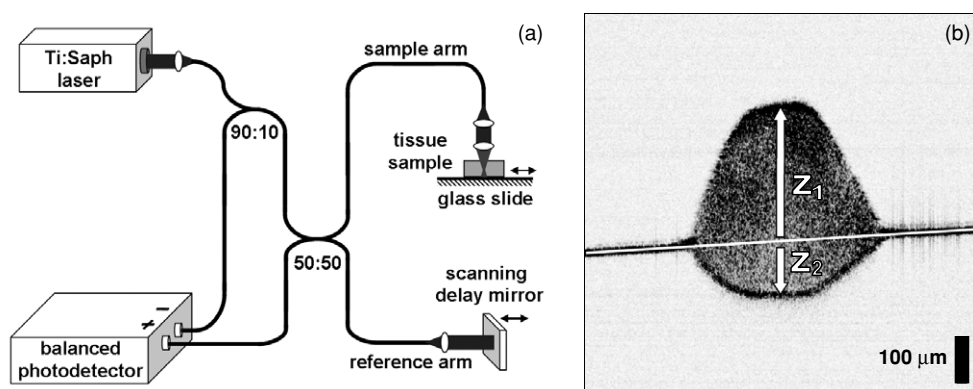


Figure 1. (a) Diagram of OCT system showing dual-balanced fibre-optic interferometer and index measurement sample arm configuration. (b) Cross-sectional OCT image of tumour tissue resting on a flat glass surface. The displacement of the otherwise flat surface (horizontal white line) below the tissue allows for the calculation of the tissue RI via measurement of z_1 and z_2 (arrows) in each image column.

image. Specifically, when the RI of the sample is greater than the free space RI in the reference arm, the depth-dependent reflections from the sample appear to be shifted away from the light source. This effect causes the apparent displacement of a reference surface (figure 1(b)), yielding curvature of the flat slide below the sample. Using the sample-free position of the slide as a reference, measurement of the distances to the top and bottom of the sample, z_1 and z_2 , respectively, allows for the computation of the refractive index via

$$n = \frac{z_1 + z_2}{z_1}. \quad (1)$$

The OCT system used in this experiment was comprised of a dual-balanced fibre-optic interferometer with a neodymium:vanadate-pumped titanium:sapphire laser source having a centre wavelength of 800 nm and approximately 100 nm of bandwidth. The system employed an achromatic sample arm lens with a 20 mm focal length, and spatial scanning in the sample arm was accomplished via a pair of x - y scanning galvanometers. The resulting system resolution was approximately $2 \mu\text{m}$ in the axial direction and $15 \mu\text{m}$ in the transverse direction. Images were spatially oversampled by at least a factor of 2, satisfying the Shannon–Nyquist sampling theorem. A galvanometer-mounted scanning mirror was used as a delay reference. Measurement of the galvanometer linearity using an autocorrelator showed that less than $0.1 \mu\text{m}$ position error was present between the actual and commanded delay-arm positions when scanning at 25 Hz. Measurement of the interferogram was accomplished via a dual-balanced photodetector with the electrical output connected to an analogue-to-digital converter and personal computer for acquisition and analysis. The final OCT image was formed after digital signal demodulation and filtering. A representative OCT image of rat tumour tissue on a glass microscope slide is shown in figure 1(b).

The OCT image of each sample was analysed using a personal computer employing specialized software. The software incorporated an edge detection scheme within user-defined image regions to measure the relevant distances for RI calculation. Each column of the image containing sample data has an associated RI value and each was treated as an individual data point. Data were extracted only from columns with a combined separation ($z_1 + z_2$) of at least 50 pixels and an incident beam angle less than 0.6 radians. These restrictions ensured

Table 1. Refractive indices of rat mammary tissue measured at a centre wavelength of 800 nm. Abbreviations: a—adipose, t—tumour, s—stroma.

Tissue type	Refractive index (mean \pm standard deviation)	Data points	$p <$ (when compared to)
Tumour	1.390 \pm 0.028	7476	0.003 (a); 1.000 (s)
Adipose	1.467 \pm 0.026	274	0.003 (t); 0.003 (s)
Fibrous stroma	1.388 \pm 0.043	219	1.000 (t); 0.003 (a)

adequate sensitivity and minimal boundary refraction effects on the optical path. In addition, an iterative algorithm was employed to compensate for refractive beampath lengthening. After initial RI calculations were completed for an image, the resulting mean RI was used to estimate the refraction of each beam based on the sample surface geometry. This refraction angle was then used to find new measures of z_1 and z_2 , and, hence, improved measurements of RI. This process was repeated until the mean RI converged to a change of less than $\Delta n = 0.001$ between iterations.

3. Results

The RI data were measured from eight rats, including one control animal with no tumours, with a total of 28 tumours. A total of 7969 data points were acquired with 274 from adipose, 219 from fibrous stroma and 7476 from tumour tissue. Table 1 shows the mean and standard deviation of the RI from each tissue type. Table 2 contains information on the size and location of each tumour, the age of the animal from which it was removed and the presence or absence of necrosis. The number of data points, mean and standard deviation of the measured data are also included in this table. Stroma and adipose tissue data were acquired from two animals (rats 1 and 3) and four animals (rats 1, 3, 4 and 5), respectively. Many stroma and adipose data were eliminated due to inhomogeneous sample composition.

The RI measurements from fibrous stroma samples had a bimodal distribution with the data centred at about 1.355 and 1.390. The modes of this distribution are correlated with an observed histological difference in the density of the H&E-stained collagen and the scattering density observed in the OCT images. It is suspected that these differences are likely the result of different collagen types, but no definitive conclusion can be reached without immunohistochemical analysis. In an effort to refine the understanding of these data, stained sections were observed under a conventional microscope using a pair of orthogonal polarizing plates positioned on either side of the sample. Both sample types were found to be highly birefringent, eliminating the possibility that they are comprised primarily of type IV collagen, which reportedly lacks the birefringence found in other collagen types due to its lack of a fibril structure (Kiernan 1999). Tumour and adipose samples were also analysed for birefringence using the same technique, and none was found. This is an expected result, but one that elucidates the possible application of birefringence sensing techniques, such as polarization sensitive OCT (PS-OCT) to the problem of differentiating between stroma and tumour tissues (Matcher *et al* 2004, Pierce *et al* 2004, Ugryumova *et al* 2005).

4. Analysis and discussion

The data show that a clear difference exists between the RI of adipose tissue and that of tumour and stroma tissues. The validity of these measurements is bolstered by the excellent statistical

Table 2. Properties of rat mammary tumours induced for the measurement of refractive index. Time post-injection is measured from the second MNU dose.

Rat tumour	Tumour size (cm)	Tumour location	Rat age/post-injection (days)	Necrosis	Data points	Refractive index (mean \pm standard deviation)
2-1	2.5	Hind limb	97/62	Yes	430	1.389 \pm 0.012
2-2	0.5	Hind limb	97/62	Yes	192	1.385 \pm 0.011
2-3	0.5	Hind limb	97/62	No	171	1.388 \pm 0.012
3-1	2.0	Hind limb	83/48	Yes	92	1.382 \pm 0.009
3-2	0.5	Fore limb	83/48	No	119	1.373 \pm 0.018
3-3	0.3	Fore limb	83/48	No	93	1.379 \pm 0.026
3-4	Nodule	Hind limb	83/48	Yes	22	1.385 \pm 0.015
4-1	2.0	Neck	81/46	No	405	1.378 \pm 0.028
4-2	1.3	Hind limb	81/46	Yes	493	1.365 \pm 0.015
4-3	0.5	Hind limb	81/46	Yes	526	1.366 \pm 0.016
5-1	1.5	Hind limb	84/49	No	126	1.372 \pm 0.019
5-2	1.5	Hind limb	84/49	No	47	1.373 \pm 0.018
5-3	1.0	Fore limb	84/49	Yes	28	1.368 \pm 0.029
5-4	0.5	Fore limb	84/49	Yes	32	1.370 \pm 0.015
5-5	0.5	Fore limb	84/49	Yes	15	1.366 \pm 0.022
5-6	0.5	Fore limb	84/49	No	70	1.376 \pm 0.024
6-1	1.2	Hind limb	82/47	Yes	170	1.371 \pm 0.013
6-2	0.8	Hind limb	82/47	Yes	250	1.369 \pm 0.017
6-3	0.4	Fore limb	82/47	No	115	1.371 \pm 0.009
6-4	Nodule	Hind limb	82/47	No	92	1.385 \pm 0.030
7-1	3.0	Hind limb	73/38	Yes	1976	1.418 \pm 0.026
8-1	1.2	Groin	90/55	No	495	1.384 \pm 0.017
8-2	1.0	Fore limb	90/55	Yes	506	1.392 \pm 0.018
8-3	1.4	Fore limb	90/55	Yes	439	1.386 \pm 0.011
8-4	1.5	Hind limb	90/55	Yes	38	1.393 \pm 0.013
8-5	2.0	Fore limb	90/55	Yes	350	1.390 \pm 0.016
8-6	Nodule	Groin	90/55	No	94	1.399 \pm 0.025
8-7	Nodule	Groin	90/55	No	87	1.393 \pm 0.021

power of these measurements. Power analysis was performed using the formula

$$\phi = \frac{\delta}{\sigma} \sqrt{\frac{p}{2k}} \quad (2)$$

for the noncentrality parameter, where δ is the minimum detectable difference between two groups, σ is the standard deviation within the population, p is the sample size and k is the number of groups (Glantz 2002). With a population standard deviation, or measurement error, of $\sigma = 0.007$ (Tearney *et al* 1995) and $k = 3$, we find that the data quantity obtained in this study yield a power of 0.99 for the detection of RI down to $\Delta n = 0.0005$ when a false-positive risk of $\alpha = 0.05$ is used. The statistical analysis performed here is based on the number of scan-line measurements due to the assumption of very high homogeneity among invasive MNU-induced lesions, as reported in the literature (Thompson *et al* 1995).

Adipose RI values that have been reported in the literature give mean values of 1.44–1.46 for subcutaneous and abdominal human fat, 1.46 for canine fat, 1.41 for subcutaneous rat

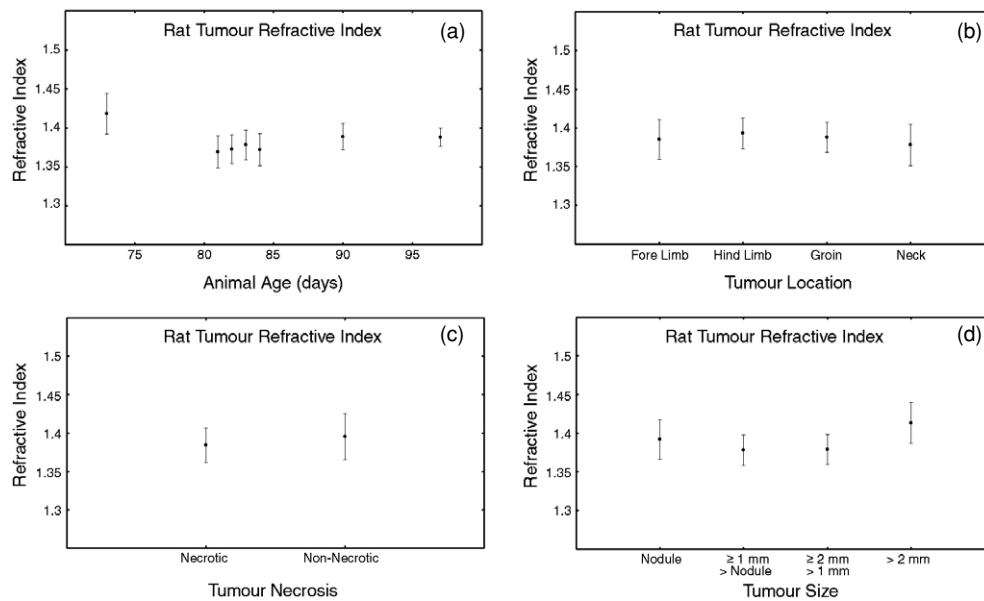


Figure 2. Refractive indices of tumour tissue grouped by (a) animal age, (b) tumour location, (c) the presence of necrosis and (d) tumour size. Error bars represent one standard deviation about the mean.

adipose, 1.493 for porcine adipose and 1.455 for bovine fat (Bolin *et al* 1989, Li and Xie 1996, Roggan *et al* 1995). The range of these values may be due in part to experimental differences in the wavelengths at which measurements were taken and the measurement devices utilized. It should especially be noted that many of the measurements reported in the literature were performed with optical sources having a much narrower spectral bandwidth than that used here. The adipose RI results shown here, having a mean of 1.467, fall within the range of these previously reported values, but are slightly higher than those previously reported for rat adipose. A limited study of two normal and malignant human breast tissue samples using a second harmonic generation technique yielded RI measurements of 1.403 and 1.431, respectively, for the two samples (Das *et al* 1997). This study, unfortunately, was purely exploratory in nature and much critical information was omitted regarding the patients from whom the samples were taken, the tissue handling techniques employed and the statistical relevance of the results. The results of this study, when compared to the RI measurements of 1.388 and 1.390 presented here, have somewhat elevated RI values. Finally, the RI of hydrated type I collagen has a reported value of 1.43, which is somewhat lower than the stroma values measured in this study (Wang *et al* 1996). This difference is likely due to the presence of other collagen types and the complex features of non-idealized tissue specimens. It should also be noted that a great deal of variation exists among the measurement techniques, radiation wavelength and tissue preparation in previously published works. In this work, the tissue was analysed *in vitro*, which could potentially differ from *in vivo* studies due to the absence of the physiological environment.

In humans, the optical properties of breast tissue are known to be dependent on blood volume and oxygenation, patient age, body mass index, hydration, menstrual cycle and disease progression (Cubeddu *et al* 2000, Durduran *et al* 2002, Shah *et al* 2004, Thomsen and Tatman 1998). In this study, information on animal age, tumour size, the presence of necrosis and

Table 3. Results of statistical analysis of variance. The comparisons correspond to the RI values in figure 2. The *p*-values below 0.05 indicate statistical significance when comparing two groups. Time post-injection is measured from the second MNU dose.

	Comparison		<i>p</i> <
Tissue	Adipose	Stroma	0.003
	Stroma	Tumour	1.000
	Tumour	Adipose	0.003
Tumour location	Fore limb	Hind limb	0.200
	Fore limb	Groin	1.000
	Fore limb	Neck	1.000
	Hind limb	Groin	1.000
	Hind limb	Neck	0.400
	Groin	Neck	1.000
Necrosis	Necrotic	Non-necrotic	0.005
Tumour size	Nodule	>Nodule, ≤1 mm	0.800
	Nodule	>1 mm, ≤2 mm	0.800
	Nodule	>2 mm	0.200
	>Nodule, ≤1 mm	>1 mm, ≤2 mm	1.000
	>Nodule, ≤1 mm	>2 mm	0.004
	>1 mm, ≤2 mm	>2 mm	0.004
Animal age (post-injection)	73 (38) days	81 (46) days	0.002
	73 (38) days	82 (47) days	0.002
	73 (38) days	83 (48) days	0.002
	73 (38) days	84 (49) days	0.002
	73 (38) days	90 (55) days	0.002
	73 (38) days	97 (62) days	0.002
	81 (46) days	82 (47) days	1.000
	81 (46) days	83 (48) days	1.000
	81 (46) days	84 (49) days	1.000
	81 (46) days	90 (55) days	0.002
	81 (46) days	97 (62) days	0.007
	82 (47) days	83 (48) days	1.000
	82 (47) days	84 (49) days	1.000
	82 (47) days	90 (55) days	0.070
	82 (47) days	97 (62) days	0.350
	83 (48) days	84 (49) days	1.000
	83 (48) days	90 (55) days	1.000
	83 (48) days	97 (62) days	1.000
	84 (49) days	90 (55) days	0.700
84 (49) days	97 (62) days	0.700	
90 (55) days	97 (62) days	1.000	

lesion location was collected for analysis. Tumour size and necrosis are important due to their relationship to the disease state, and animal age is indicative of maturity, a factor that is often studied in human disease. Finally, tumour location information was compiled in order to substantiate our assumption that all lesions are of the same pathological origin. The data were grouped by these parameters and statistical power calculation and analysis of variance were performed. Figure 2 shows the RI values in relation to animal age, the size and location of the tumours and the presence of necrosis. The statistical power to detect the minimum mean differences (0.0004, 0.0013, 0.0024, 0.0114) between any two data sets in the size, age,

location and necrosis comparisons is 0.72, <0.5, 0.99 and 0.99, respectively. Clearly, any conclusion drawn from the animal age data presented here should be greatly tempered by the low statistical power.

Analysis of variance was performed as a means of statistically interpreting the tissue type comparison between tumour, fibrous stroma and adipose as well as the comparisons among tumour properties. The *t*-test was used for the two-group comparison of necrosis and the Bonferroni *t*-test was used for the other comparisons. These analyses yielded the *p*-values shown in table 3, which represent the probability that the two groups being compared were taken from the same population (i.e. no statistical difference exists between the two groups). The results demonstrate that the RI of adipose tissue is significantly different from that of fibrous stroma and tumour tissues but that no differentiation can be made between stroma and tumour samples. The analysis also shows that no significant difference exists based on tumour location, supporting the interpretation that position-dependent pathological variation was absent among the tumours.

Lesion size, animal age and the presence of necrosis also have some effect on RI of tumour samples. Specifically, statistical significance exists when tumours larger than 2 mm in size are compared with other lesions, except in the case of small nodules, defined as palpable lesions less than 500 μm in size. The higher RI of late-stage tumours is likely due to the pathological progression of the disease relative to other lesions. The exception being small tumour nodules, the RI of which may be influenced by the lack of extensive angiogenic vasculature present in more mature tumours. While the *p*-values also suggest that some tumour RI variation exists among animals of different age, these results are limited. The youngest rat in this study was euthanized at 73 days of age, more than 1 week before any other animal, and was found to have a single, large tumour. Therefore, the significant variation present in this tumour sample could be due to a number of factors, including the elevated RI found in larger lesions. Beyond the RI from the first animal, only two other comparisons yield a significant result based on age, rats aged 82 days compared with those 90 and 97 days of age. A more comprehensive study is necessary before any significant deduction can be made from such a limited variation based on animal age. Finally, the presence of necrosis has a significant effect, yielding a somewhat lower RI than in non-necrotic tumour samples.

While the developmental, pathological and chemical similarities between human breast ductal carcinoma and MNU-induced rat mammary tumours have been experimentally shown, some differences may still exist. Furthermore, as mentioned previously, *in vivo* and *in vitro* optical measurements often yield different properties. The measurement of *in vitro* tissue from an animal model has, however, been used extensively in the past. While the analysis of human tissue is still necessary, these results offer a basis on which to develop an improved understanding of breast tissue properties.

5. Conclusion

The RI values from 28 MNU-induced rat mammary tumours, which are well known to correspond to ductal carcinomas in humans, are shown to have a mean value of 1.390. While similar to the RI of some fibrous stroma tissues, a significant difference exists between tumour and adipose values. As in many of the known optical parameters of the human breast, some variations also exist in the RI of rat tumours based on parameters indicative of the disease state. These previously unreported values present an opportunity for more accurate modelling of the diffusion process that governs photon migration through the breast and may potentially yield optimized tomographic breast imagery. The RI difference between adipose tissue, which comprises the vast majority of the breast, and tumour tissue may also open the possibility for

a range of RI detection techniques to be applied to the optical diagnosis of breast disease, including the possible use of interferometric ranging techniques for real-time surgical guidance and pathological evaluation.

Acknowledgments

The authors acknowledge Freddy Nguyen and Wei Luo for their assistance with animal handling and Dr Amy Oldenburg, Dr Claudio Vinegoni and John Fahrner for their work on the development and maintenance of the measurement system. We thank Dr Keith Singletary from the Department of Food Science and Human Nutrition at the University of Illinois at Urbana-Champaign for his insight and assistance with this animal tumour model. This work was supported in part by funding from the National Institutes of Health (NIBIB, 1 R01 EB00108-1, SAB) and the UIUC-UIC Intercampus Research Initiative in Biotechnology (SAB).

References

- Alexandrov S A, Zvyagin A V, Silva K K and Sampson D D 2003 Bifocal optical coherence refractometry of turbid media *Opt. Lett.* **28** 117–9
- Anderson C H and Beattie C W 1992 Cellular kinetics of rat mammary gland terminal end bud epithelium exposed to *N*-methyl-*N*-nitrosourea *in vivo* *Cancer Res.* **52** 5076–81
- Arafah B M, Finegan H M, Roe J, Manni A and Pearson O H 1982 Hormone dependency in *N*-nitrosomethylurea-induced rat mammary tumors *Endocrinology* **111** 584–8
- Arafah B M, Gullino P M, Manni A and Pearson O H 1980 Effect of ovariectomy on hormone receptors and growth of *N*-nitrosomethylurea-induced mammary tumors in the rat *Cancer Res.* **40** 4628–30
- Arridge S R 1999 Optical tomography in medical imaging *Inverse Problems* **15** R41–93
- Bartsch H, Nair J and Owen R W 1999 Dietary polyunsaturated fatty acids and cancers of the breast and colorectum: emerging evidence for their role as risk modifiers *Carcinogenesis* **20** 2209–18
- Bigsby R M 2002 Synergistic tumor promoter effects of estrone and progesterone in methylnitrosourea-induced rat mammary cancer *Cancer Lett.* **179** 113–9
- Bolin F P, Preuss L E, Taylor R C and Ference R J 1989 Refractive index of some mammalian tissues using a fiber optic cladding method *Appl. Opt.* **28** 2297–303
- Boppart S A, Luo W, Marks D L and Singletary K W 2004 Optical coherence tomography: feasibility for basic research and image-guided surgery of breast cancer *Breast Cancer Res. Treat.* **84** 85–97
- Cerussi A E, Berger A J, Bevilacqua F, Shah N, Jakubowski D, Butler J, Holcombe R F and Tromberg B J 2001 Sources of absorption and scattering contrast for near-infrared optical mammography *Acad. Radiol.* **8** 211–8
- Chan M M, Lu X, Merchant F M, Iglehart J D and Miron P L 2005 Gene expression profiling of NMU-induced rat mammary tumors: cross species comparison with human breast cancer *Carcinogenesis* **26** 1343–53
- Chang M, Liu H and Jordan V C 2002 *Cancer of the Breast* ed W L Donegan and J S Spratt (New York: Saunders) pp 417–41
- Chernomordik V, Hattery D W, Grosenick D, Wabnitz H, Rinneberg H, Moesta K T, Schlag P M and Gandjbakhche A 2002 Quantification of optical properties of a breast tumor using random walk theory *J. Biomed. Opt.* **7** 80–7
- Clarke R 1996 Animal models of breast cancer: their diversity and role in biomedical research *Breast Cancer Res. Treat.* **39** 1–6
- Clarke R 1997 Animal models of breast cancer: experimental design and their use in nutrition and psychosocial research *Breast Cancer Res. Treat.* **46** 117–33
- Cohen L A, Thompson D O, Maeura Y, Choi K, Blank M E and Rose D P 1986 Dietary fat and mammary cancer: I. Promoting effects of different dietary fats on *N*-nitrosomethylurea-induced rat mammary tumorigenesis *J. Natl Cancer Inst.* **77** 33–42
- Crist K A, Chaudhuri B, Shivaram S and Chaudhuri P K 1992 Ductal carcinoma *in situ* in rat mammary gland *J. Surg. Res.* **52** 205–8
- Cubeddu R, D'Andrea C, Pifferi A, Taroni P, Torricelli A and Valentini G 2000 Effects of the menstrual cycle on the red and near-infrared optical properties of the human breast *Photochem. Photobiol.* **72** 383–91
- Das B B, Liu F and Alfano R R 1997 Time-resolved fluorescence and photon migration studies in biomedical and model random media *Rep. Prog. Phys.* **60** 227–92

- Dehghani H, Brooksby B A, Pogue B W and Paulsen K D 2005 Effects of refractive index on near-infrared tomography of the breast *Appl. Opt.* **44** 1870–8
- Dehghani H, Brooksby B, Vishwanath K, Pogue B W and Paulsen K D 2003 The effects of internal refractive index variation in near-infrared optical tomography: a finite element modelling approach *Phys. Med. Biol.* **48** 2713–27
- Domankevitz Y, Waldman J, Lin C P and Anderson R R 2000 Selective delivery of laser energy to biological tissue based on refractive-index differences *Opt. Lett.* **25** 1104–6
- Dulbecco R, Armstrong B, Allen W R and Bowman M 1986 Distribution of developmental markers in rat mammary tumors induced by *N*-nitrosomethylurea *Cancer Res.* **46** 5144–52
- Durduran T, Choe R, Culver J P, Zubkov L, Holboke M J, Giammarco J, Chance B and Yodh A G 2002 Bulk optical properties of healthy female breast tissue *Phys. Med. Biol.* **47** 2847–61
- Fantini S, Walker S A, Franceschini M A, Kaschke M, Schlag P M and Moesta K T 1998 Assessment of the size, position, and optical properties of breast tumors *in vivo* by noninvasive optical methods *Appl. Opt.* **37** 1982–9
- Fay M P, Freedman L S, Clifford C K and Midthune D N 1997 Effect of different types and amounts of fat on the development of mammary tumors in rodents: a review *Cancer Res.* **57** 3979–88
- Ferwerda H A 1999 The radiative transfer equation for scattering media with a spatially varying refractive index *J. Opt. A: Pure Appl. Opt.* **1** L1–2
- Gibson A P, Hebden J C and Arridge S R 2005 Recent advances in diffuse optical imaging *Phys. Med. Biol.* **50** R1–43
- Glantz S A 2002 *Primer of Biostatistics* (New York: McGraw-Hill)
- Green A, Shilkaitis A and Christov K 1999 4-(Hydroxyphenyl)retinamide selectively inhibits the development and progression of ductal hyperplastic lesions and carcinoma *in situ* in mammary gland *Carcinogenesis* **20** 1535–40
- Grosenick D, Wabnitz H, Moesta K T, Mucke J, Moller M, Stroszczynski C, Stossel J, Wassermann B, Schlag P M and Rinneberg H 2004 Concentration and oxygen saturation of haemoglobin of 50 breast tumours determined by time-domain optical mammography *Phys. Med. Biol.* **49** 1165–81
- Gullino P M, Pettigrew H M and Grantham F H 1975 *N*-nitrosomethylurea as mammary gland carcinogen in rats *J. Natl Cancer Inst.* **54** 401–14
- Hill M, Bausero M, Mazal D, Menoret S, Khalife J, Anegon I and Osinaga E 2004 Immunobiological characterization of *N*-nitrosomethylurea-induced rat breast carcinomas: tumoral IL-10 expression as a possible immune escape mechanism *Breast Cancer Res. Treat.* **84** 107–16
- Iftimia N V, Bouma B E, Pitman M B, Goldberg B, Bressner J and Tearney G J 2005 A portable, low coherence interferometry based instrument for fine needle aspiration biopsy guidance *Rev. Sci. Instrum.* **76** 064301
- Jin Z, Houle B, Mikheev A M, Cha R S and Zarbl H 1996 Alterations in H-ras1 promoter conformation during *N*-nitroso-*N*-methylurea-induced mammary carcinogenesis and pregnancy *Cancer Res.* **56** 4927–35
- Kiernan J A 1999 *Histological and Histochemical Methods* (New York: Oxford University Press)
- Li H and Xie S 1996 Measurement method of the refractive index of biotissue by total internal reflection *Appl. Opt.* **35** 1793–5
- Lu J, Pei H, Kaeck M and Thompson H J 1997 Gene expression changes associated with chemically induced rat mammary carcinogenesis *Mol. Carcinog.* **20** 204–15
- Luo W, Nguyen F T, Zysk A M, Ralston T S, Brockenbrough J, Marks D L, Oldenburg A L and Boppart S A 2005 Optical biopsy of lymph node morphology using optical coherence tomography *Technol. Cancer Res. Treat.* **4** 539–48
- Markel V A and Schotland J C 2005 Multiple projection optical diffusion tomography with plane wave illumination *Phys. Med. Biol.* **50** 2351–64
- Martí-López L, Bouza-Domínguez J, Hebden J C, Arridge S R and Martínez-Celorio R A 2003 Validity conditions for the radiative transfer equation *J. Opt. Soc. Am. A* **20** 2046–56
- Matcher S J, Winlove C P and Gangnus S V 2004 The collagen structure of bovine intervertebral disc studied using polarization-sensitive optical coherence tomography *Phys. Med. Biol.* **49** 1295–306
- McCormick D L, Adamowski C B, Fiks A and Moon R C 1981 Lifetime dose-response relationships for mammary tumor induction by a single administration of *N*-methyl-*N*-nitrosourea *Cancer Res.* **41** 1690–4
- Moon R C, Grubbs C J, Sporn M B and Goodman D G 1977 Retinyl acetate inhibits mammary carcinogenesis induced by *N*-methyl-*N*-nitrosourea *Nature* **267** 620–1
- Ohmi M, Ohnishi Y, Yoden K and Haruna M 2000 *In vitro* simultaneous measurement of refractive index and thickness of biological tissue by the low coherence interferometry *IEEE Trans. Biomed. Eng.* **47** 1266–70
- Peters V G, Wyman D R, Patterson M S and Frank G L 1990 Optical properties of normal and diseased human breast tissues in the visible and near infrared *Phys. Med. Biol.* **35** 1317–34
- Pierce M C, Sheridan R L, Park B H, Cense C and Boer J F d 2004 Collagen denaturation can be quantified in burned human skin using polarization-sensitive optical coherence tomography *Burns* **30** 511–7
- Roggan A, Dörschel K, Minet O, Wolff D and Muller G 1995 *Laser-Induced Interstitial Thermotherapy* (Bellingham, WA: SPIE)

- Rose D P, Fischer A H and Jordan V C 1981 Activity of the antioestrogen trioxifene against *N*-nitrosomethylurea-induced rat mammary carcinomas *Eur. J. Cancer Clin. Oncol.* **17** 893–8
- Schweiger M, Gibson A and Arridge S R 2003 Computational aspects of diffuse optical tomography *Comput. Sci. Eng.* **5** 33–41
- Shah N, Cerussi A E, Jakubowski D, Hsiang D, Butler J and Tromberg B J 2004 Spatial variations in optical and physiological properties of healthy breast tissue *J. Biomed. Opt.* **9** 534–40
- Singh M, McGinley J N and Thompson H J 2000 A comparison of the histopathology of premalignant and malignant mammary gland lesions induced in sexually immature rats with those occurring in the human *Lab. Invest.* **80** 221–31
- Sinha D K, Pazik J E and Dao T L 1983 Progression of rat mammary development with age and its relationship to carcinogenesis by a chemical carcinogen *Int. J. Cancer* **31** 321–7
- Sorin W V and Gray D F 1992 Simultaneous thickness and group index measurement using optical low-coherence reflectometry *IEEE Photonics Technol. Lett.* **4** 105–7
- Tearney G J, Brezinski M E, Southern J F, Bouma B E, Hee M R and Fujimoto J G 1995 Determination of the refractive index of highly scattering human tissue by optical coherence tomography *Opt. Lett.* **20** 2258–60
- Thompson H J 1997 Effects of physical activity and exercise on experimentally-induced mammary carcinogenesis *Breast Cancer Res. Treat.* **46** 135–41
- Thompson H J and Adlakha H 1991 Dose-responsive induction of mammary gland carcinomas by the intraperitoneal injection of 1-methyl-1-nitrosourea *Cancer Res.* **51** 3411–5
- Thompson H J, Adlakha H and Singh M 1992 Effect of carcinogen dose and age at administration on induction of mammary carcinogenesis by 1-methyl-1-nitrosourea *Carcinogenesis* **13** 1535–9
- Thompson T A, Haag J D and Gould M N 2000a *ras* gene mutations are absent in NMU-induced mammary carcinomas from aging rats *Carcinogenesis* **21** 1917–22
- Thompson H J, McGinley J N, Knott K K, Spoelstra N S and Wolfe P 2002 Vascular density profile of rat mammary carcinomas induced by 1-methyl-1-nitrosourea: implications for the investigation of angiogenesis *Carcinogenesis* **23** 847–54
- Thompson H J, McGinley J N, Rothhammer K and Singh M 1995 Rapid induction of mammary intraductal proliferations, ductal carcinoma *in situ* and carcinomas by the injection of sexually immature female rats with 1-methyl-1-nitrosourea *Carcinogenesis* **16** 2407–11
- Thompson H J, McGinley J, Rothhammer K and Singh M 1998 Ovarian hormone dependence of pre-malignant and malignant mammary gland lesions induced in pre-pubertal rats by 1-methyl-1-nitrosourea *Carcinogenesis* **19** 383–6
- Thompson H J, Singh M and McGinley J 2000b Classification of premalignant and malignant lesions developing in the rat mammary gland after injection of sexually immature rats with 1-methyl-1-nitrosourea *J. Mammary Gland Biol. Neoplasia* **5** 201–10
- Thomsen S and Tatman D 1998 Physiological and pathological factors of human breast disease that can influence optical diagnosis *Ann. New York Acad. Sci.* **838** 171–93
- Thordarson G, Lee A V, McCarty M, Van Horn K, Chu O, Chou Y C, Yang J, Guzman R C, Nandi S and Talamantes F 2001 Growth and characterization of *N*-methyl-*N*-nitrosourea-induced mammary tumors in intact and ovariectomized rats *Carcinogenesis* **22** 2039–47
- Tualle J-M and Tinet E 2003 Derivation of the radiative transfer equation for scattering media with a spatially varying refractive index *Opt. Commun.* **228** 33–8
- Ugryumova N, Attenburrow D P, Winlove C P and Matcher S J 2005 The collagen structure of equine articular cartilage, characterized using polarization-sensitive optical coherence tomography *J. Phys. D: Appl. Phys.* **38** 2612–9
- Wang X-J, Milner T E, Chang M C and Nelson J S 1996 Group refractive index measurement of dry and hydrated type I collagen films using optical low-coherence reflectometry *J. Biomed. Opt.* **1** 212–6
- Wang X, Zhang C, Zhang L, Xue L and Tian J 2002 Simultaneous refractive index and thickness measurements of bio tissue by optical coherence tomography *J. Biomed. Opt.* **7** 628–32
- Welsch C W 1992 Relationship between dietary fat and experimental mammary tumorigenesis: a review and critique *Cancer Res.* **52** 2040s–2048s
- Zvyagin A V, Dilusha Silva K K M B, Alexandrov S A, Hillman T R, Armstrong J J, Tsuzuki T and Sampson D D 2003 Refractive index tomography of turbid media by bifocal optical coherence refractometry *Opt. Express* **11** 3503–17
- Zysk A M and Boppart S A 2006 Human breast cancer identification by k-space analysis of optical coherence tomography images *Biomedical Optics 2006 Technical Digest* (Washington, DC: Optical Society of America) SH14
- Zysk A M, Reynolds J J, Marks D L, Carney P S and Boppart S A 2003 Projected index computed tomography *Opt. Lett.* **28** 701–3